Received: 23 September 2022 | Revised: 4 November 2022 | Accepted: 7 November 2022

DOI: 10.1002/mrc.5324

RESEARCH ARTICLE

WILEY

J-modulated ^{19}F- and ^{1}H-detected dual-optimized inverted $^{1}J_{CC}$ 1,n-ADEQUATE: A universal ADEQUATE experiment

Ronald C. Crouch[1] | **Marius Pelmuş**[2] | **Jeffrey G. Raab**[3,4] | **Evgeny Tischenko**[1] | **Michael Frey**[1] | **Yunyi Wang**[5] | **Mikhail Reibarkh**[5] | **R. Thomas Williamson**[3] | **Gary E. Martin**[2]

[1]Analytical Instruments, JEOL USA Inc., Peabody, Massachusetts, USA

[2]Department of Chemistry, Seton Hall University, South Orange, New Jersey, USA

[3]Department of Chemistry and Biochemistry, University of North Carolina Wilmington, Wilmington, North Carolina, USA

[4]Department of Chemistry and Chemical Biology, Stevens Institute of Technology, Hoboken, New Jersey, USA

[5]Analytical Research and Development, Merck and Co., Inc., Rahway, New Jersey, USA

Correspondence
Gary E. Martin, Department of Chemistry, Seton Hall University, 400 South Orange Ave., South Orange, NJ, USA.
Email: gemartin.mrc@gmail.com

Present address
Jeffrey G. Raab, Department of Chemistry and Chemical Biology, Stevens Institute of Technology, Hoboken, New Jersey, USA.

Abstract

The recently reported ^{19}F-detected dual-optimized inverted $^{1}J_{CC}$ 1,n-ADEQUATE experiment and the previously reported ^{1}H-detected version have been modified to incorporate *J*-modulation, making it feasible to acquire all 1,1- and 1,n-ADEQUATE correlations as well as $^{1}J_{CC}$ and $^{n}J_{CC}$ homonuclear scalar couplings in a single experiment. The experiments are demonstrated using *N,N*-dimethylamino-2,5,6-trifluoro-3,4-phthalonitrile and *N,N*-dimethylamino-3,4-phthalonitrile.

KEYWORDS

1,1-ADEQUATE, 1,n-ADEQUATE, ^{19}F-detection, ^{1}H-detection, $^{1}J_{CC}$, dual-optimization, inverted $^{1}J_{CC}$ correlations, *J*-modulation, $^{n}J_{CC}$

1 | INTRODUCTION

When investigators encounter an especially challenging structure elucidation problem, they may be forced to resort to more sophisticated experimental methods. Several examples of this approach to the solution of otherwise intractable structure problems can be cited. The structure of the spirononacyclic alkaloid cryptospirolepine, first reported in 1993,[1] was found to have been erroneously assigned in 2002 when several degradation products were characterized, one of which could not be mechanistically rationalized from the originally reported structure.[2] It took another 13 years until the development of TCI MicroCryoProbe™ capabilities[3] and homonuclear decoupled (HD) ADEQUATE techniques became available before the remaining submilligram sample could be fully characterized in 2015.[4] The characterization of homodimericin-A is another pertinent example.[5] As recounted by Professor Jon Clardy at an American Society of Pharmacognosy meeting,[6] the molecule, which has a C_{20} central core containing 14 non-protonated carbons, 11 of them contiguous, refused to crystallize and also defied structural characterization using conventional two-dimensional nuclear magnetic resonance spectroscopy (2D NMR) techniques, even when supplemented by computer-assisted structure

elucidation (CASE) methods, for more than 3 years because of the ambiguity of long-range heteronuclear correlation pathways in heteronuclear multiple-bond correlation experiments. In contrast, when 1,1-HD-ADEQUATE data were employed, it took less than 2 weeks to solve the structure. A third example is found in the elucidation of the breitfussin structure, which defied characterization by 2D NMR supplemented by CASE methods.[7] That impasse prompted the first reported utilization of atomic force microscopy (AFM) to characterize the substitution of what was shown to be an iodo-oxazole ring. Since that first report, there has been substantial progress in the development of anisotropic NMR methods, which several of the authors demonstrated could be used to unequivocally assign another breitfussin analog in 2019.[8]

Poly- and perfluorinated environmental pollutants, like the aforementioned examples, can also represent significant structure characterization challenges. In our continuing efforts to surmount such challenges, we recently reported the development of ^{19}F-detected variants[9,10] of the ADEQUATE experiment[11] that can be utilized for the characterization of poly- and perfluoro compounds when sufficient samples are available. Our more recent report[10] embodied the dual-optimization scheme of the inverted $^{1}J_{CC}$ 1,n-ADEQUATE experiment capable of inverting $^{1}J_{CC}$ correlations across a broad range of potential $^{1}J_{CC}$ scalar coupling constants, thereby allowing both $^{1}J_{CC}$ and $^{n}J_{CC}$ correlations to be measured in a single experiment.[11,12] Now, we report the further extension of the dual-optimization protocol with *J*-modulation[13–15] for both ^{19}F- and ^{1}H-detected ADEQUATE experiments allowing the establishment and differentiation of $^{1}J_{CC}$ and $^{n}J_{CC}$ correlations with simultaneous measurement of $^{1}J_{CC}$ and $^{n}J_{CC}$ scalar homonuclear scalar coupling constants. To facilitate comparison, the ^{19}F-detected experiment was performed on *N,N*-dimethylamino-2,5,6-trifluoro-3,4-phthalonitrile (**1**) employed in previous studies,[9,10] whereas the ^{1}H-detected experiments were performed on *N,N*-dimethylamino-3,4-phthalonitrile (**2**) (the numbering scheme is the same for both molecules).

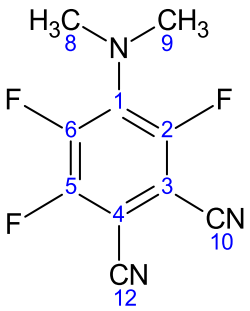

1

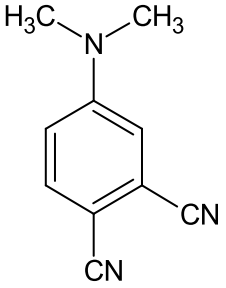

2

The *J*-modulated variants of the experiment employ the pulse sequence shown in Figure 1, where the "X" trace can be either ^{19}F or ^{1}H. The dual-optimization scheme employed for ^{19}F-detection is identical to that contained in the previous paper.[10] The red-boxed segment of the pulse sequence corresponds to the *J*-scaling module of the experiment, whereas the blue-boxed regions provide the dual optimization that affords broadband inversion of the $^{1}J_{CC}$ correlations.

One of the inherent problems associated with poly- and perfluorinated molecules is the impact of the highly electronegative fluorine atoms on the size of the $^{1}J_{CC}$ and $^{n}J_{CC}$ homonuclear coupling constants. Although an investigator would typically optimize the delays for the $^{1}J_{CC}$ coupling constant in a conventional ^{1}H-detected 1,1-ADEQUATE experiment in the range of about 50 Hz, which we have shown previously is a reasonable compromise between aryl and alkyl carbon–carbon coupling constants,[16–18] this is not a viable optimization for per- and polyfluorinated molecules. For a conventional ^{19}F-detected 1,1-ADEQUATE spectrum of *N,N*-dimethylamino-2,5,6-trifluoro-3,4-phthalonitrile (**1**), it was necessary to optimize the delays to 80 Hz to obtain good quality data.[9,10] In the same sense, it was necessary to reoptimize parameters for the delays for a ^{19}F-detected dual-optimized inverted $^{1}J_{CC}$ 1,n-ADEQUATE experiment.[10] One of the typical sets of optima for ^{1}H-detected dual-optimized inverted $^{1}J_{CC}$ 1,n-ADEQUATE experiments, 57.0/9.5 and 64.0/8.0 Hz for the $^{1}J_{CC}/^{n}J_{CC}$ delay pairings, is graphically shown in Figure S1.[12,13] As is immediately apparent, the blue summation curve affords near zero to slightly positive intensity for $^{1}J_{CC}$ coupling constants in a range of 80–90 Hz. Although a ^{19}F-detected experiment using these delay optimizations would provide some data, $^{1}J_{CC}$ correlations could in some cases be absent or positive. In contrast, as shown in the two panels of Figure S2, paired optima of 58.0/6.5 and 80.0/6.5 Hz (panel A) and 70.0/10.0 and 83.0/11.5 Hz (panel B) for the $^{1}J_{CC}/^{n}J_{CC}$ delay pairings affords inversion of $^{1}J_{CC}$ correlations across a range from 37.7–95.7 and 43.0–100.3 Hz, respectively. This range is consistent with the $^{1}J_{CC}$ coupling constants of **1** measured using an INADEQUATE experiment.[9]

2 | ^{19}F-DETECTED *J*-MODULATED DUAL-OPTIMIZED INVERTED $^{1}J_{CC}$ 1,N-ADEQUATE

Using the pulse sequence shown in Figure 1 with the *J*-modulation module turned off, coupled with the delay optimizations reported previously (see Figure S2B),[10]

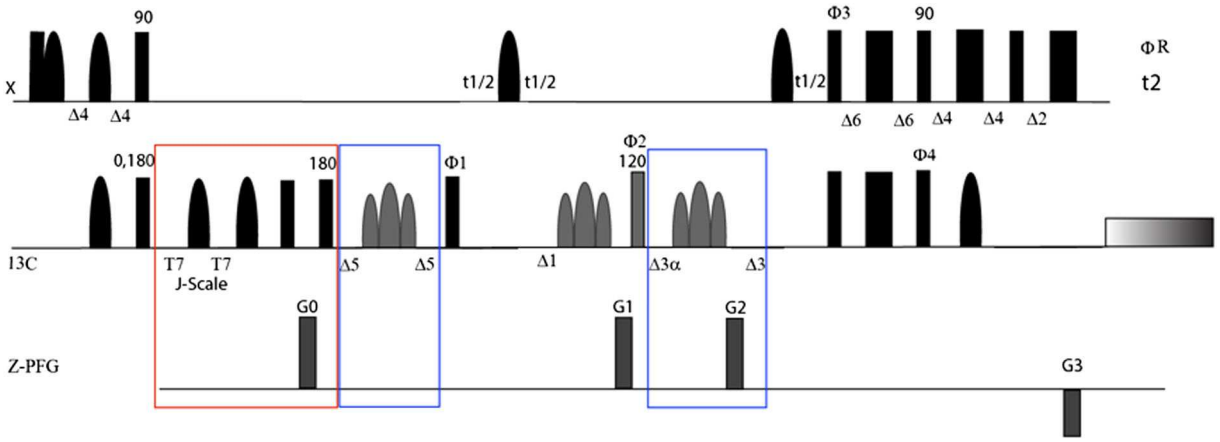

FIGURE 1 ADEQUATE pulse sequence for X-nucleus detection (X = ^{1}H or ^{19}F) with the addition of *J*-modulation module (red boxed segment) after the first X → ^{13}C INEPT transfer. Dual optimization (blue boxed segments) is achieved by interleaving on alternate scans between the chosen two *J* optimizations shown as Δ5–^{13}C Chirp Δ5 along with Δ3a through Δ3. Based on the desire to co-add all of the data, the normal ADEQUATE phase cycle was doubled. For example, 0° 0° 180° 180° was extended to become 0° 0° 0° 0° 180° 180° 180° 180°, etc. The sequence shown was further modified from the normal ADEQUATE pulse sequence by replacing simple X square 180° pulses (either ^{1}H or ^{19}F depending on which nuclide is being observed) with BIP 720-100-10 constructs to significantly increase effective inversion bandwidth to accommodate the chemical shift range of ^{19}F. Phases are denoted in the figure with the extended 32-step phase cycle. Φ1 = 8 (0°), 8(180°) with incrementation by 180° on odd t_1 increments; Φ2 = 16(0°), 16(180°); Φ3 = 4(0°), 4(180°); Φ4 = 4(90°), 4(270°) for one of the P- and N-type phases and 4(270°), 4(90°) for the other as the decoding PFG pulse, G3, is inverted. Receiver phase, ΦR = 2(0°), 4(180°), 2 (0°), 2(180°), 4(0°), 4(180°), 4(0°), 2(180°), 2(0°), 4(180°), 2(0°) with incrementation by 180° on odd t_1 increments. Any pulse unlabeled with a phase value is phase = 0°. Gradient ratios for the experiment were G0 = homospoil; G1 = 77.4; G2 = 78.5; and G3 = 59.0 for ^{1}H and for ^{19}F, the gradient ratios were G0 = homospoil; G1 = 77.4; G2 = 78.5; G3 = 62.7. The amplitude transfer curves for ^{1}H and ^{19}F are shown in Figures S1 and S2, respectively. (Pulse sequence codes for JEOL delta and Bruker instruments are included in the Supporting Information).

the data shown in Figure 2 were obtained for **1**. As is apparent from an inspection of the spectrum, all of the anticipated 1,1- and 1,n-ADEQUATE responses are observed with the correct phase.

The experiment was repeated with the *J*-modulation component of the pulse sequence enabled and the *J*-scaling factor set to 24 to ensure that $^{n}J_{CC}$ correlations would be sufficiently upscaled to ensure that they were readily and accurately measurable. Typically for a *J*-modulated 1,1-ADEQUATE experiment, a scaling factor of 10 would suffice; for the typical *J*-modulated 1,n-ADEQUATE experiment, a scaling factor of 30 would be used. Setting the scaling factor to 24 was an effective compromise. The data from the *J*-modulated dual-optimized inverted $^{1}J_{CC}$ 1,n-ADEQUATE spectrum are shown in Figure 3, and an expansion of the correlations for the F5 resonance is presented in Figure 4 to better illustrate the detail in the spectrum. The J_{CC} coupling constants measured from the data presented in Figure 3 were completely comparable with those measured previously for this compound as determined from a ^{13}C INADEQUATE experiment.[10]

3 | ISOTOPE SHIFTS

Isotope shifts are not often a point of modern-day discussion; hence, it is interesting to recall that Ramsey first predicted the occurrence of them in 1952,[19] followed by an experimental demonstration of the phenomenon by Wimett in 1953.[20] One of the early reviews on the topic was produced by Batiz-Hernandez and Bernheim in 1963[21] followed by the review of Jameson in 2007.[22] More recently, Hansen has reviewed the isotope effects on chemical shifts in the study of tautomerism[23] and intramolecular hydrogen bonds.[24] Other recent reviews have appeared but are not germane to small molecule investigations. There have also been several studies reported that utilize $^{35/37}$Cl isotope shifts by Molinski's group[25,26] and the NMR group at Merck & Co., Inc.[27,28] Very recently, Hwang and coworkers[29] have reported the observation $^{35/35}$Cl isotope shifts on ^{15}N resonances in the case of N → Cl bonds in the course of a structure elucidation study. An ancillary benefit of the *J*-modulated dual-optimized inverted $^{1}J_{CC}$ 1,n-ADEQUATE experiment is that isotope shifts can be readily measured

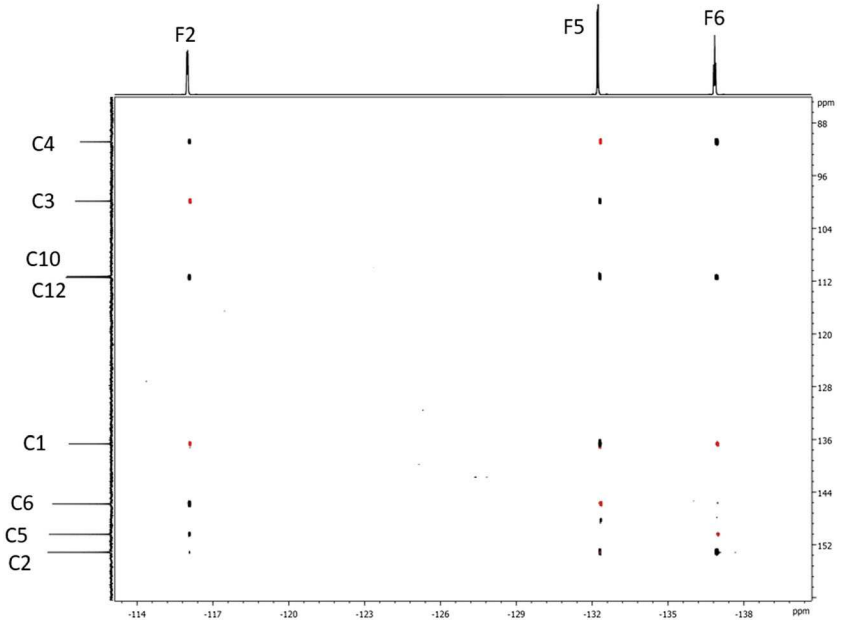

FIGURE 2 ^{19}F-detected dual-optimized inverted $^{1}J_{CC}$ 1,n-ADEQUATE spectrum of *N,N*-dimethylamino-2,5,6-trifluoro-3,4-phthalonitrile (**1**) using the pulse sequence shown in Figure 1 with the *J*-modulation feature of the pulse sequence turned off. The data were acquired as 96 t_1 increments with 1536 transients/increment with 50% NUS sampling, giving an acquisition time of 67 h. The final resolution after the NUS extension was 0.42 ppm. The dual-optimization pairs were 70.0/10.0 and 83.0/11.5 Hz. The spectrum is identical to that reported previously using the previously reported dual-optimized version of the experiment that did not utilize the *J*-modulation module.[10] $^{1}J_{CC}$ Correlations are inverted and plotted in red, whereas $^{n}J_{CC}$ correlations have positive intensity and are plotted in black. The delays are all internally calculated by the sequence based on the input pairs noted above. $\Delta 5 = 24.0$ ms for even scans and 20.08434 ms for odd scans. $\Delta 3a = 16.85714$ ms for even scans and 14.06024 ms for odd scans. $\Delta 3 = 15.38978$ ms for even scans and 12.59288 ms for odd scans. INEPT delays based on a 250 Hz $^{1}J_{CF}$ value.

from the data. Comparatively speaking, measurement of isotope shifts will be somewhat facilitated in the non-*J*-modulated experiment since the inherent signal-to-noise ratio of that experiment will be somewhat higher than that in the *J*-modulated variant in which the signal intensity is split between the limbs of the doublet in the F1 frequency domain. There also exists the possibility that isotope shifts, when measured, can be used as a means of identifying the occasional $^{2}J_{CC}$ or $^{3}J_{CC}$ correlation observed in a 1,1-ADEQUATE experiment.[30–32]

4 | ^{1}H-DETECTED *J*-MODULATED DUAL-OPTIMIZED INVERTED $^{1}J_{CC}$ 1,N-ADEQUATE

As was noted in the introduction, the *J*-modulated dual-optimized inverted $^{1}J_{CC}$ 1,n-ADEQUATE experiment can be used for ^{1}H as well as the ^{19}F detection experiment. The ^{1}H-detected data were acquired using the *N,N*-dimethylamino-3,4-phthalonitrile (**2**) to facilitate comparison with the fluorinated congener. Aside from selecting for ^{1}H rather than ^{19}F detection (with associated gradient ratio changes), it is also necessary to select a dual-optimization pairing appropriate for the size of the $^{1}J_{CC}$ homonuclear coupling constants of protonated compounds. The dual-optimized inverted $^{1}J_{CC}$ 1, n-ADEQUATE spectrum of **2** is shown in Figure 5; the data were acquired with dual-optimization pairs of 57/9.5 and 64/8 Hz with the *J*-modulation turned off. The spectrum shown in Figure 6 was acquired with the *J*-modulation module employed. The scaling factor was set to 24 to ensure that both the $^{1}J_{CC}$ and $^{n}J_{CC}$ doublets would be sufficiently upsized to allow all of the homonuclear carbon–carbon coupling constants to be accurately measured. An expansion of the correlations for the H5 resonance is shown in Figure 7.

The $^{1}J_{CC}$ and $^{n}J_{CC}$ homonuclear coupling constants for **2** extracted from the spectrum shown in Figure 6 are collected in Table 2. Despite the congestion in the ^{13}C spectrum in the region of 115–119 ppm, it was still possible to extract those coupling constants successfully. Although isotope shifts were expected for the ^{19}F-detected variant of the experiment performed on **1** based on our previous work,[10] it is interesting to note that small (ranging from 1 to 4 ppb) but measurable isotope shifts were also observed in the ^{1}H-detected data. To the best of our knowledge, this is the first time that isotope

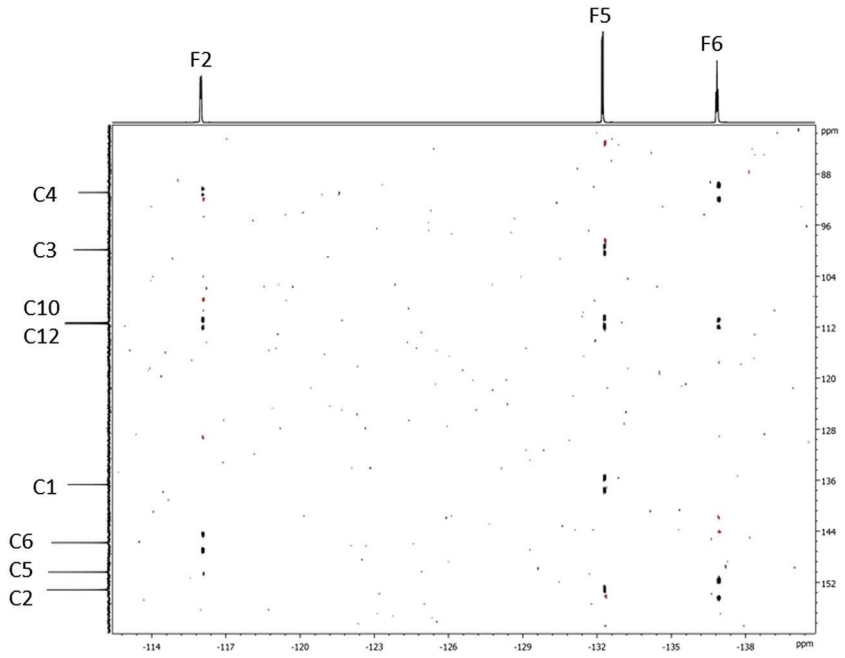

FIGURE 3 ^{19}F-detected *J*-modulated dual-optimized inverted $^{1}J_{CC}$ 1,n-ADEQUATE spectrum of *N,N*-dimethylamino-2,5,6-trifluoro-3,4-phthalonitrile (**1**) acquired using the pulse sequence shown in Figure 1 with the *J*-modulation feature enabled, and with the scaling factor set to 24. The data were acquired as 224 t_1 increments with 1536 transients/increment with 50% NUS sampling, giving an acquisition time of 92 h. The final F1 resolution was 22 Hz after the NUS extension before taking into account the *J*-scaling factor of 24X. As would be expected, splitting the correlations into multiplets in the F1 dimension reduces the relative sensitivity of the experiment as compared with data acquired when the *J*-modulation module is not employed (see Figure 1). The dual-optimization pairs were 70.0/10.0 and 83/11.5 Hz. $^{1}J_{CC}$ Correlations are inverted and appear as doublets in the F1 domain and are plotted in red, whereas $^{n}J_{CC}$ correlations have positive intensity and are plotted in black. In a full-scale plot, it is difficult to see the doublets for smaller long-range carbon–carbon couplings or the isotope effects inherent to the correlations that we reported previously.[9,10] However, these features of the experiment are prominent in the expansion of the correlations for the F5 resonance shown in Figure 4 (expansions for the F2 and F6 resonances are presented in the Supporting Information). All delays are exactly as noted in Figure 2.

shifts have been noted and measured from the ^{1}H-detected ADEQUATE spectrum.

It is quite likely that because of the small size of these isotope shifts, they were overlooked previously or that investigators simply aligned the correlations observed in the 2D contour plot with the reference spectra, which is a routine practice, thereby obliterating the isotope shift information extant in the data. The diminutive size of the isotope shifts (1–4 ppb) is consistent with the difference between the chemical shift ranges of ^{1}H and ^{19}F, which play a large role in the size of the observed isotope shifts,[18] ^{19}F-detected spectra affording isotope shifts that range from 77 to 108 ppb for **1** using the same experiment.

Not anticipating the observation of isotope shifts associated with correlations in the ^{1}H-detected experiment, no effort was made to acquire these data with precision high enough to accurately measure the tiny isotope shifts that ranged from ≈1 to 4 ppb. Further studies are ongoing in an effort to measure the isotope shifts observable in ^{1}H-detected ADEQUATE experiments with greater precision. That work will be the subject of a future communication.

5 | COUPLING CONSTANT COMPARISONS

Although the $^{1}J_{CC}$ and $^{n}J_{CC}$ homonuclear coupling constants for **1** and **2** are presented in Tables 1 and 2, respectively, there is rarely an opportunity to directly compare coupling constants between a compound and its perfluoro analog. Thus, we thought it would be beneficial to extract the corresponding coupling constants and to directly contrast the various homonuclear scalar coupling constants as shown in Figure 8. As is readily apparent from Figure 8, on average, the $^{1}J_{CC}$ scalar coupling constants from the fluoro analog, **1**, average approximately 30% larger than the corresponding coupling constants from the protonated molecule, **2**, except for the C5-C6 $^{1}J_{CC}$ coupling constant, for which the difference is even larger. It is interesting to note that for the $^{2}J_{CC}$ and the $^{3}J_{CC}$ long-range coupling constants, there are substantial disparities between the protio and fluoro analogs; the basis for which is not immediately clear. These observations suggest that developing a more detailed understanding of the effect of fluorination on the magnitude of

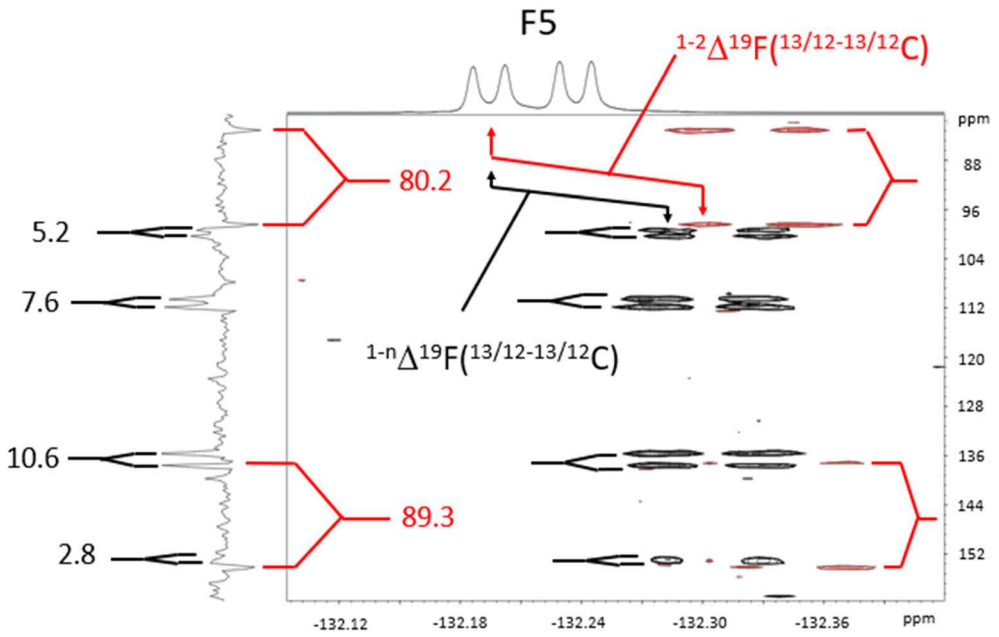

FIGURE 4 Expansion of the F5 correlations from the ^{19}F-detected *J*-modulated dual-optimized inverted $^{1}J_{CC}$ 1,n-ADEQUATE spectrum of **1** acquired with optimization pairs of 70.0/10.0 and 83.0/11.5 Hz (see Figure S2B). Data are plotted with the inverted $^{1}J_{CC}$ correlations shown in red and the long-range $^{n}J_{CC}$ correlations in black. Doublets in the F1 dimension for both types of correlations are upscaled by K = 24 to allow accurate measurement of both the $^{1}J_{CC}$ and $^{n}J_{CC}$ coupling constants. Isotope shifts inherent to the ^{19}F-detected ADEQUATE experiment are denoted using the convention from our previous work and are summarized in Table 1.[10] Values for the coupling constants shown were obtained by dividing the measured F1 splitting by the scaling factor, K.

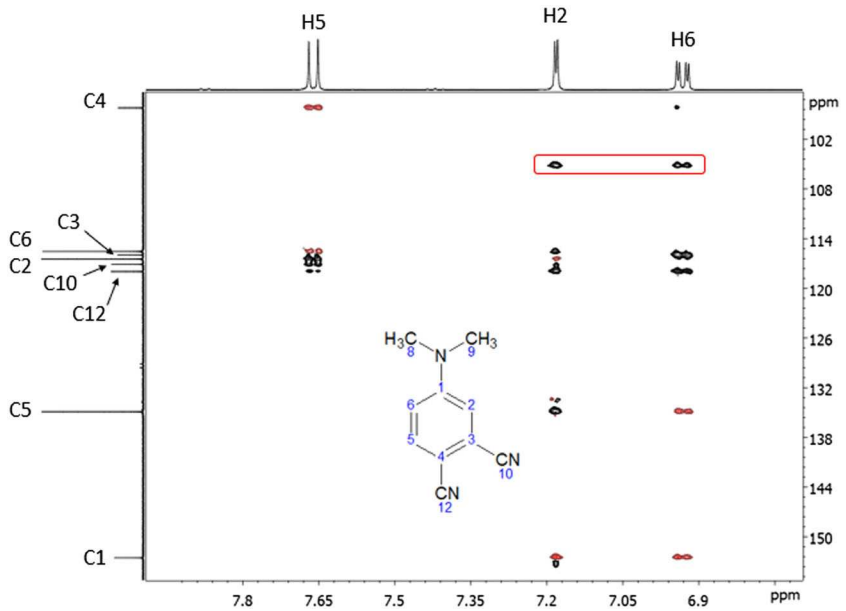

FIGURE 5 Dual-optimized inverted $^{1}J_{CC}$ 1,n-ADEQUATE spectrum of *N,N*-dimethylamino-3,4-phthalonitrile (**2**) acquired using the pulse sequence shown in Figure 1 with the *J*-modulation module turned off. The data were acquired in 12 h 10 m at 40°C as 48 t_1 increments (50% NUS) with 256 transients for each accumulated increment; 96 t_1 increments were acquired across 80 ppm of ^{13}C yielding after NUS extension a final resolution of 0.42 ppm. The ^{1}H acquisition time was 0.25539 s with a relaxation delay of 1.4 s. The dual-optimization pairs were 57/9.5 and 64/8 Hz. The $^{1}J_{CH}$ delays were optimized for 160 Hz. Correlations in the red-boxed region arise from the folded F1 responses associated with the *N,N*-dimethylamino group. All delays were internally calculated by the pulse sequence based on the input pairs noted above. Δ5 = 29.70175 ms for even scans and 34.15626 ms for odd scans. Δ3a = 20.92982 ms for even scans and 26.34375 ms for odd scans. Δ3 = 19.50682 ms for even scans and 24.92075 ms for odd scans. INEPT delays based on a J_{HC} = 160 Hz.

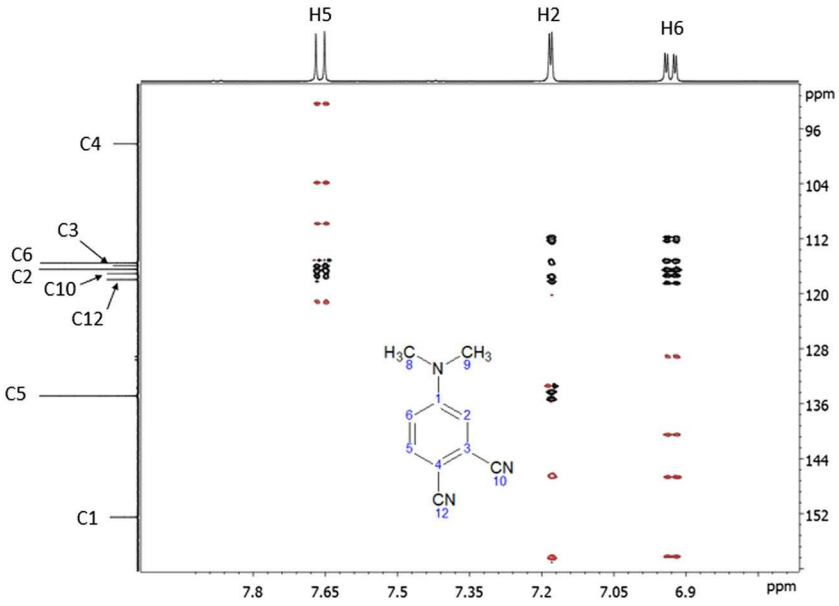

FIGURE 6 *J*-modulated dual-optimized inverted $^{1}J_{CC}$ 1, n-ADEQUATE spectrum of *N,N*-dimethylamino-3,4-phthalonitrile (**2**) acquired using the pulse sequence shown in Figure 1 with the *J*-modulation module enabled. The dual-optimization pairs were 57/9.5 and 64/8 Hz. The scaling factor was set to 24 to ensure that the $^{1}J_{CC}$ and $^{n}J_{CC}$ coupling constants could be accurately measured. An expansion of the correlations for the H5 resonance is shown in Figure 7. The ^{1}H acquisition time was 0.25539 s with a 1.75-s relaxation delay with 640 scans accumulated for 224 t1 increments at 50% NUS, with an acquisition time of 82 h 15 m. The final F1 resolution was 22 Hz before taking into account the 24X *J*-scaling factor. All delays are exactly as noted in Figure 5.

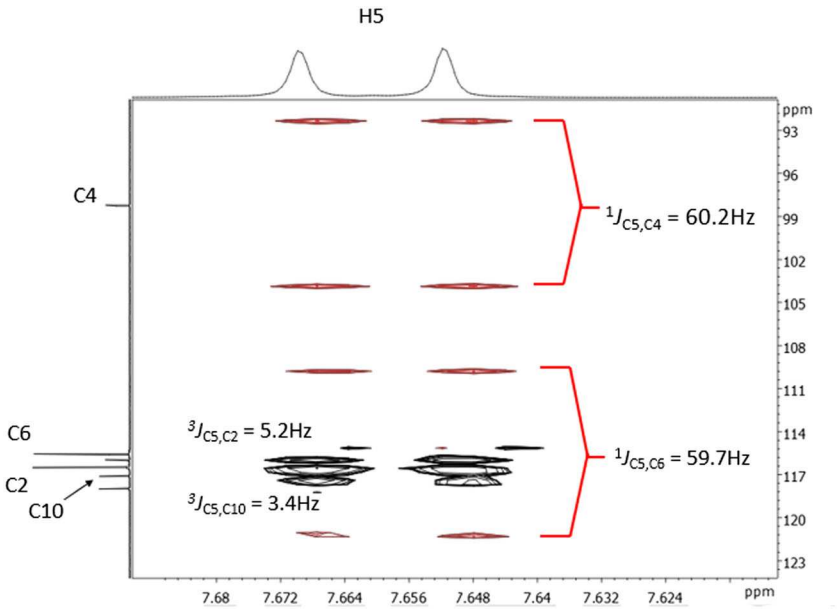

FIGURE 7 Expansion of the region of the spectrum of the *J*-modulated dual-optimized inverted $^{1}J_{CC}$ 1,n-ADEQUATE spectrum of **2** from Figure 6. When plotted on this scale, small isotope shifts ranging from ≈ 1 to 4 ppb are observable and could be roughly measured (see Table 2). Values for the coupling constants shown were again obtained by dividing the measured F1 splitting by the scaling factor, K.

J_{CC} coupling constants would be important for optimal NMR parameter setting and data interpretation in the course of structure elucidation of perfluorinated organic compounds and environmental pollutants.

6 | EXPERIMENTAL

All NMR data were acquired using either a 53-mg sample of *N,N*-dimethylamino-2,5,6-trifluoro-3,4-phthalonitrile

TABLE 1 Homonuclear scalar coupling constants ($^{1}J_{CC}$ and $^{n}J_{CC}$) and isotope shifts measured from the *J*-modulated dual-optimized inverted $^{1}J_{CC}$ 1,n-ADEQUATE spectrum of *N,N*-dimethylamino-2,5,6-trifluoro-3,4-phthalonitrile (**1**) shown in Figure 3 recorded using the pulse sequence shown in Figure 1 with the dual-optimization pairs set to 70.0/10.0 and 83.0/11.5 Hz. Measured coupling constants were comparable with those measured using a ^{13}C INADEQUATE experiment

	F2			F5			F6		
Carbon	$^{1}J_{CC}$ (Hz)	$^{n}J_{CC}$ (Hz)	$^{1-n}\Delta^{19}F$ ($^{13/12-13/12}C$) (ppb)[a]	$^{1}J_{CC}$ (Hz)	$^{n}J_{CC}$ (Hz)	$^{1-n}\Delta^{19}F$ ($^{13/12-13/12}C$) (ppb)[a]	$^{1}J_{CC}$ (Hz)	$^{n}J_{CC}$ (Hz)	$^{1-n}\Delta^{19}F$ ($^{13/12-13/12}C$) (ppb)[a]
1	76.7		$^{1-2}\Delta$, −107		10.3	$^{1-3}\Delta$, −85	78.7		$^{1-2}\Delta$, −99
2					7.8	$^{1-3}\Delta$, −89			$^{1-3}\Delta$, −79
3	82.6		$^{1-2}\Delta$, −108		5.6			14.3	$^{1-4}\Delta$, −77
4		5.7	$^{1-3}\Delta$, −85	80.5		$^{1-2}\Delta$, −109		12.1	$^{1-3}\Delta$, −78
5			$^{1-4}\Delta$, −85				89.8		
6		14.1	$^{1-3}\Delta$, −85	89.3		$^{1-2}\Delta$, −111			$^{1-2}\Delta$, −78
10-C ≡ N					7.1	$^{1-4}\Delta$, −80			
12-C ≡ N		6.9	$^{1-4}\Delta$, −79		2.8			5.9	$^{1-4}\Delta$, −76

[a]The isotope shifts are designated as $^{1-n}\Delta$ where $n = 2$ denotes a vicinal $^{1}J_{CC}$ correlation (1,1-ADEQUATE) isotope shift and where $n = 3$ denotes a $^{2}J_{CC}$ and $n = 4$ denotes a $^{3}J_{CC}$ 1,n-ADEQUATE correlation isotope shift. The ADEQUATE correlation pathways are shown in the structure below:

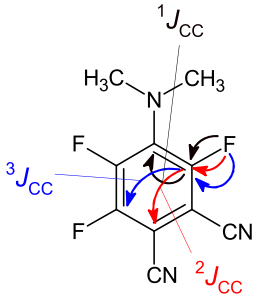

TABLE 2 Homonuclear scalar coupling constants ($^{1}J_{CC}$ and $^{n}J_{CC}$) and isotope shifts measured from the *J*-modulated dual-optimized inverted $^{1}J_{CC}$ 1,n-ADEQUATE spectrum of *N,N*-dimethylamino-3,4-phthalonitrile (**2**) shown in Figure 6 recorded using the pulse sequence shown in Figure 1 with the dual-optimization pairs set to 57.0/9.5 and 64.0/8.0 Hz. Measured coupling constants were again comparable with those measured using a ^{13}C INADEQUATE experiment

	H2			H5			H6		
Carbon	$^{1}J_{CC}$ (Hz)	$^{n}J_{CC}$ (Hz)	$^{1-n}\Delta^{1}H$ ($^{13/12-13/12}C$) (ppb)[a]	$^{1}J_{CC}$ (Hz)	$^{n}J_{CC}$ (Hz)	$^{1-n}\Delta^{1}H$ ($^{13/12-13/12}C$) (ppb)[a]	$^{1}J_{CC}$ (Hz)	$^{n}J_{CC}$ (Hz)	$^{1-n}\Delta^{1}H$ ($^{13/12-13/12}C$) (ppb)[a]
1	62.0		$^{1-2}\Delta$, −4				60.5		$^{1-2}\Delta$, −3
2					5.2				
3	n.o.					$^{1-3}\Delta$, −2		6.9	$^{1-3}\Delta$, −1
4		2.9		60.2		$^{1-2}\Delta$, −3		2.8	
5		5.2	$^{1-4}\Delta$, −2				58.8		$^{1-2}\Delta$, −4
6		≈1.9	$^{1-3}\Delta$, −2	59.7		$^{1-2}\Delta$, −4			
8/9 Me		2.7	$^{1-4}\Delta$, −2					2.5	$^{1-4}\Delta$, −1
10-C ≡ N					3.4	$^{1-4}\Delta$, −3			$^{1-4}\Delta$, −1
12-C ≡ N		3.9	$^{1-4}\Delta$, −2		2.1			5.7	$^{1-4}\Delta$, −1

Abbreviation: n.o., not observed.

[a]The isotope shifts are designated as $^{1-n}\Delta$ where $n = 2$ denotes a vicinal $^{1}J_{CC}$ correlation (1,1-ADEQUATE) isotope shift and where $n = 3$ denotes a $^{2}J_{CC}$ and $n = 4$ denotes a $^{3}J_{CC}$ 1,n-ADEQUATE correlation isotope shift. The ADEQUATE correlation pathways are shown in the structure below. We estimate the accuracy of the isotope shift measurement to be on the order of ±0.5 to 1.0 ppb (see text).

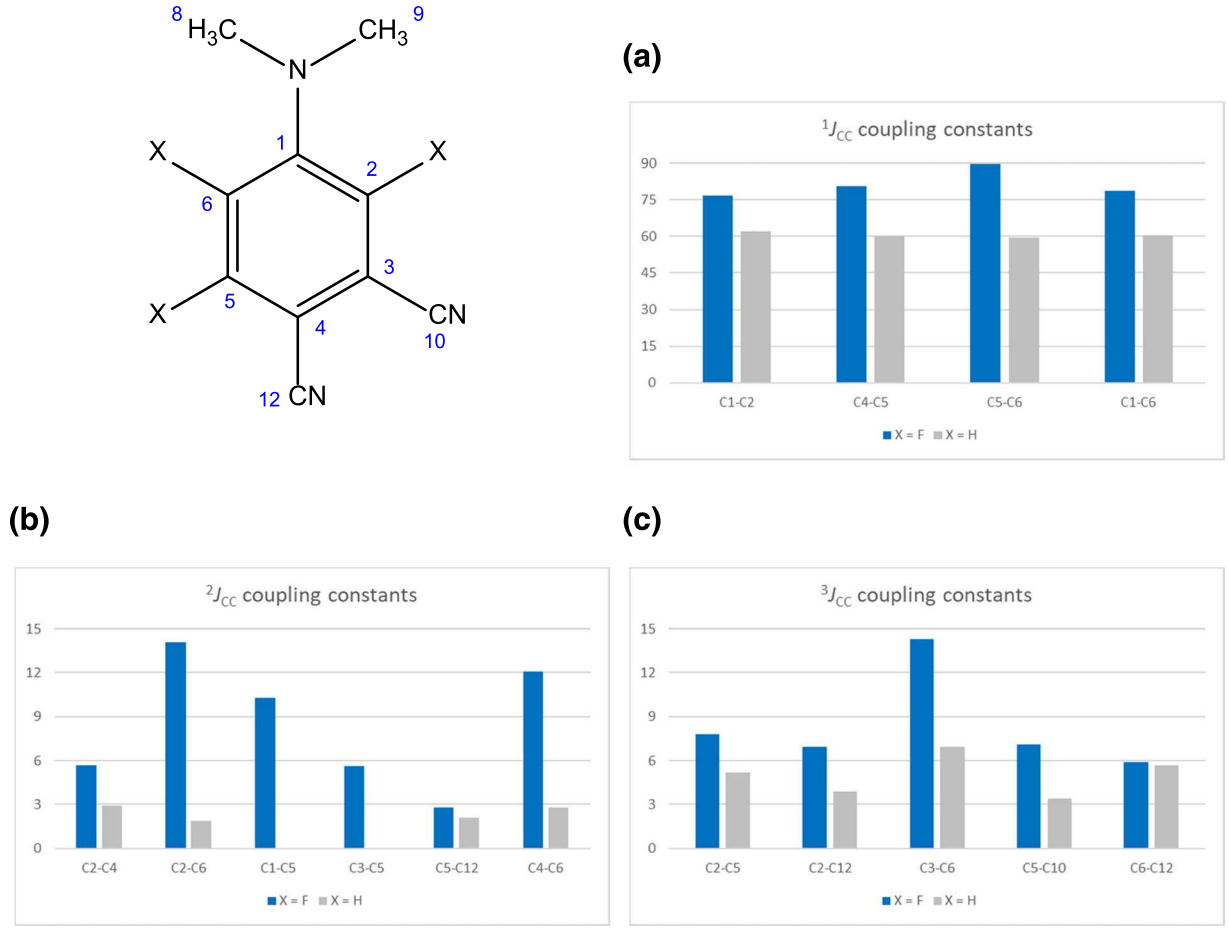

FIGURE 8 Graphical comparison of the $^{1}J_{CC}$, $^{2}J_{CC}$, and $^{3}J_{CC}$ homonuclear scalar coupling constants from **1** and **2**. Coupling constants for the fluorinated compound **1** are shown in blue, whereas for the protio compound **2** are shown in grey. The coupling constant values used to generate the figure are present in Table S1. There is no provision in the experiment shown in Figure 1 for determining the relative sign of the $^{2}J_{CC}$ and $^{3}J_{CC}$ homonuclear coupling constants.

(**1**)[33] or a 50-mg sample of *N,N*-dimethylamino-3,4-phthalonitrile (**2**)[34] dissolved in 550 µl of DMSO-d_6.[1] Concentrated samples were employed to facilitate data analysis and the generation of publication quality data; less concentrated samples can be employed for routine analysis. Data were acquired using a JEOL ECZ500R spectrometer equipped with a SuperCOOL™ broadband probe. Parameters for individual experiments are provided in the figure captions. All data were processed with matched Gaussian window functions in both dimensions after doubling the acquired F1 points as part of the NUS reconstruction process. Additional experimental details are included in figure captions. Plots were prepared using the JEOL JASON software package 1.2.2669. JEOL Delta 6 and Bruker pulse sequence codes for the *J*-modulated dual-optimized inverted $^{1}J_{CC}$ 1,n-ADEQUATE experiment are provided in the Supporting Information.

7 | CONCLUSIONS

In conclusion, we have demonstrated that the ^{19}F-detected dual-optimized inverted $^{1}J_{CC}$ 1,n-ADEQUATE experiment, which we previously reported, can be further modified to incorporate a *J*-modulation module that allows the simultaneous measurement of $^{1}J_{CC}$ and $^{n}J_{CC}$ homonuclear coupling constants from a single experiment. In this report, it was also shown that the approach is also amenable to ^{1}H-detected experiments. Consequently, ^{1}H- and ^{19}F-detected experiments afforded a direct comparison of $^{1}J_{CC}$ and $^{n}J_{CC}$ coupling constants for protio and fluoro analogs of the model compound. The results demonstrated that fluorination leads to significant increases in the magnitude of $^{1}J_{CC}$, $^{2}J_{CC}$, and $^{3}J_{CC}$ coupling constants despite model compounds having an identical carbon skeleton. Isotope shifts in the ^{19}F data were consistent with those reported previously,[10] and

we report for the first time small but measurable isotope shifts ranging from ≈1 to 4 ppm for correlations in the ^{1}H-detected variant of the experiment. These diminutive isotope shifts have likely been overlooked previously by investigators, including ourselves, when 2D contour plots are routinely aligned with the 1D reference spectra plotted flanking the contour plots during data processing. As noted above, further work is ongoing in an effort to more accurately measure the minuscule isotope shifts associated with correlations in ^{1}H-detected ADEQUATE experiments, which will be the subject of a future communication.

ACKNOWLEDGMENTS

The authors wish to acknowledge the support of JEOL USA for providing generous access to NMR systems used to acquire the data in this report and the Center for Functional Materials from Seton Hall University for providing the reagents needed in the synthesis.

ORCID

R. Thomas Williamson https://orcid.org/0000-0001-7450-3135
Gary E. Martin https://orcid.org/0000-0003-0750-3041

REFERENCES

[1] A. N. Tackie, G. L. Boye, M. H. M. Sharaf, P. L. Schiff Jr., R. C. Crouch, T. D. Spitzer, R. L. Johnson, J. Dunn, D. Minick, G. E. Martin, *J. Nat. Prod.* **1993**, *56*, 653.

[2] G. E. Martin, C. E. Hadden, D. J. Russell, B. D. Kaluzny, J. E. Guido, W. K. Duholke, B. A. Stiemsma, T. J. Thamann, R. C. Crouch, K. Blinov, M. Elyashberg, E. R. Martirosian, S. G. Molodotsov, A. J. Williams, P. L. Schiff Jr., *J. Heterocyclic Chem.* **2002**, *39*, 1241.

[3] a) R. Triebe, R. Nast, D. Marek, R. Withers, L. Baselikgia, M. Haeberli, T. Gerfin, and P. Calderon, 'A User-Friendly System for the Routine Application of Cryogenic NMR Probes: Technology and Results', 40th Experimental NMR Conference, Orlando FL, Feb 28–Mar 5, 1999, Abst. W&Th, p. 201; b). J. Pease, R. Withers, R. Nast, A. Deese, P. Calderon, M. Saumil, T. Kelly, and F. Laukein, 'Application of a 2.5-mm CryoProbe to Metabolite Studies', 40th Experimental NMR Conference, Orlando FL, Feb 28–Mar 5, 1999, Abst. W&Th, p. 202; c) C. Richter, D. Marek, M. Haebeli, L. Baseligia, O. Schett, R. Triebe, D. Moskau, New Applications for Triple Resonance Cryogenic High-Resolution NMR Probes, in *41st Experimental NMR Conference*, Abstr. W&Th, Asilomar, CA, April 9–14 **2000** 153. d) D. J. Russell, C. E. Hadden, G. E. Martin, A. A. Gibson, A. P. Zens, J. L. Carolan, *J. Nat. Prod.* **2000**, *63*, 1047. e) R. C. Crouch, W. Llanos, K. G. Mehr, D. J. Russell, C. E. Hadden, G. E. Martin, *Magn. Reson. Chem* **2001**, *39*, 555.

[4] J. Saurí, W. Bermel, A. V. Buevich, M. H. M. Sharaf, P. L. Schiff Jr., T. Parella, R. T. Williamson, G. E. Martin, *Angew. Chem., Int. Ed.* **2015**, *54*, 10160.

[5] E. Mevers, J. Saurí, Y. Liu, A. Moser, T. R. Ramadhar, M. Varlan, R. T. Williamson, G. E. Martin, J. Clardy, *J. Am. Chem. Soc.* **2016**, *138*, 12324.

[6] Remarks by Professor Jon Clardy at the 60th American Society of Pharmacognosy Annual Meeting, Madison, Wisconsin, July 13-17 (**2019**).

[7] K. Ø. O. Hanssen, B. Schuler, A. J. Williams, T. B. Demissie, E. Hansen, J. H. Andersen, J. Svenson, K. Blinov, M. Repisky, F. Mohn, G. Meyer, J.-S. S. Svendsen, K. Ruud, M. Elyashberg, L. Gross, M. Jaspars, J. Isaksson, *Angew. Chem., Int. Ed.* **2012**, *51*, 12238.

[8] I. E. Ndukwe, Y.-H. Lam, S. K. Pandey, B. E. Haug, A. Bayer, E. C. Sherer, K. A. Blinov, R. T. Williamson, J. Isaksson, M. Reibarkh, Y. Liu, G. E. Martin, *Chem. Sci.* **2020**, *11*, 2081.

[9] J. Raab, M. Pelmus, G. E. Martin, R. C. Crouch, E. Tishcenko, M. Frey, R. T. Williamson, A. V. Buevich, M. Reibarkh, *Magn. Reson. Chem.* **2021**, *59*, 628.

[10] R. Crouch, J. Raab, M. Pelmus, E. Tischenko, M. Frey, A. V. Buevich, M. Reibarkh, R. T. Williamson, G. E. Martin, *Magn. Reson. Chem.* **2022**, *60*, 210.

[11] M. Köck, B. Rei, W. Fenical, C. Griesinger, *Tet. Lett.* **1996**, *37*, 363.

[12] G. E. Martin, K. A. Blinov, M. Reibarkh, R. T. Williamson, *Magn. Reson. Chem.* **2012**, *50*, 722.

[13] M. Reibarkh, R. T. Williamson, G. E. Martin, W. Bermel, *J. Magn. Reson.* **2013**, *236*, 126.

[14] B. Reif, M. Köck, R. Kerssebaum, J. Schleucher, C. Griesinger, *J. Magn. Reson.* **1996**, *B112*, 295.

[15] K. Kövér, P. Forgó, *J. Magn. Reson.* **2004**, *166*, 47.

[16] G. E. Martin, Using 1,1- and 1,n-ADEQUATE 2D NMR Data in Structure Elucidation Protocols, in *Ann. Rep. NMR Spectrosc*, (Ed: G. A. Webb) Vol. 74, Elsevier, London **2011** 215.

[17] G. E. Martin, M. Reibarkh, A. V. Buevich, K. A. Blinov, R. T. Williamson, *eMagRes* **2014**, *3*, 215. https://doi.org/10.1002/9780470034590.emrstm1370

[18] J. Saurí, I. E. Nudukwe, M. Reibarkh, Y. Liu, R. T. Williamson, G. E. Martin, *Ann. Rep. NMR Spectrosc.* **2019**, *98*, 1. https://doi.org/10.1016/bs.arnmr.2019.04.001

[19] N. F. Ramsey, *Phys. Rev.* **1952**, *87*, 1075.

[20] T. F. Wimett, *Phys. Rev.* **1953**, *91*, 476.

[21] H. Batiz-Hernandez, R. A. Bernheim, *Prog. In Nucl. Magn. Reson. Spectrosc.* **1963**, *3*, 63.

[22] C. J. Jameson, *Encycl. NMR* **2012**, *4*, 2197. previously published in *eMagnReson* 2007 DOI: 10:1002:9780470034590.emrstm0251

[23] P. E. Hansen, *Tautomerism* **2014**, 145.

[24] P. E. Hansen, *Molecules* **2015**, *20*, 2405.

[25] X. Wang, B. M. Duggan, T. F. Molinski, *J. Am. Chem. Soc.* **2015**, *2015*(137), 12343.

[26] X. Wang, B. M. Duggan, T. F. Molinski, *Magn. Reson. Chem.* **2017**, *55*, 263.

[27] J. Saurí, M. Reibarkh, T. Zhang, R. D. Cohen, X. Wang, T. F. Molinski, G. E. Martin, R. T. Williamson, *Org. Lett.* **2016**, *18*, 4786.

[28] D. J. Milanowski, N. Oku, L. K. Carter, H. R. Bokesh, R. T. Williamson, J. Saurí, Y. Liu, K. A. Blinov, Y. Ding, X.-C. Li, D. Ferreira, L. A. Walker, S. Khan, M. T. Davies-Coleman, J. A.

Kelley, J. B. McMahon, G. E. Martin, K. R. Gustafson, *Chem. Sci.* **2018**, *9*, 307.
[29] T.-L. Hwang, N. Yang, G. Cheng, Y. Chen, S. Cui, *Magn. Reson. Chem.* **2022**, *60*, 157.
[30] J. Saurí, Y. Liu, R. T. Williamson, G. E. Martin, *Magn. Reson. Chem.* **2016**, *54*, 341.
[31] R. D. Cohen, J. Saurí, C. A. Huff, S. W. Krska, G. E. Martin, *Magn. Reson. Chem.* **2016**, *54*, 897.
[32] H.-Y. Kim, J. Saurí, R. D. Cohen, G. E. Martin, *Magn. Reson. Chem.* **2018**, *56*, 775.
[33] M. Pelmuş, J. G. Raab, H. H. Patel, C. Colomier, R. I. I. I. Foglia, S. P. Kelty, S. M. Gorun, *J. Porphyrins Phthalocyanines* **2021**, *25*, 224.
[34] S. A. Mikhalenko, V. M. Derkacheva, E. A. Luk'yanets, *Zh. Obshch. Khim.* **1981**, *51*, 1650.

SUPPORTING INFORMATION

Additional supporting information can be found online in the Supporting Information section at the end of this article.

How to cite this article: R. C. Crouch, M. Pelmuş, J. G. Raab, E. Tischenko, M. Frey, Y. Wang, M. Reibarkh, R. T. Williamson, G. E. Martin, *Magn Reson Chem* **2023**, *61*(3), 169. https://doi.org/10.1002/mrc.5324